Acta Cryst. (1967). **23**, 693

Seemann–Bohlin X-Ray Diffractometry. II. Comparison of Aberrations and Intensity with Conventional Diffractometer*

BY M. MACK AND W. PARRISH

Philips Laboratories, Briarcliff Manor, New York 10510, *U.S.A.*

(*Received* 30 *December* 1966)

Geometrical expressions, graphs and experimental data for several specimen aberrations (radial and angular displacement, flat specimen and transparency) and intensity are compared for the Seemann–Bohlin (S–B) and conventional (*c*) diffractometers. The broadening and shift of the profiles are generally larger in the S–B. The integrated intensity ratio of the variable receiving aperture S–B/*c* decreases from 14 at 20°2θ to 3 at 100°, and the ratio of the constant aperture S–B/*c* increases from 2 at 20° to 5 at 40° and remains constant at higher θ's. The relative merits of the diffractometers are evaluated.

The principles of a Seemann–Bohlin (S–B) counter tube diffractometer are described in an accompanying paper (Parrish & Mack, 1967); this paper employs the same notation. The pertinent expressions and experimental data are presented in this paper to illustrate and confirm the magnitude of the various geometrical factors for the aberrations that originate in the specimen, and the intensity. The data are compared with those obtained using a conventional (*c*) diffractometer (Wilson, 1963; Parrish, 1965). Segmüller (1957) derived intensity formulae and expressions for the shift of the centroid and line broadening. Segmüller & Wincierz (1959) used the S–B with focusing crystal monochromator to measure lattice parameters for determining stress relief time in Fe–Cu alloys. Kunze (1964) published extensive papers in which he derived similar expressions which included higher order terms.

Except as specifically noted the experimental data reported below were obtained under the following experimental conditions: Cu anode X-ray tube with line focus 0·04 by 8 mm at $\psi = 6°$, 40 kV peak-to-peak full-wave rectification, 0·018 mm thick Ni filter (when used), variable receiving aperture with $W_{RS} = 0{\cdot}076$ mm, $W_{AS} = 2{\cdot}03$ mm, two sets of parallel slits with $\delta = 4{\cdot}5°$, axial length of incident assembly 12 mm and receiving assembly 20 mm, $R = R_c = 174$ mm, $\gamma = 15°$, scintillation counter with pulse amplitude discrimination, scan speed $\frac{1}{8}°4\theta$ min^{-1}, time constant 1 sec, chart speed 60 in.hr^{-1}.

Specimen aberrations in the focusing plane

The ideal condition for proper focusing is obtained when the diffracting crystallites lie exactly on the focusing circle *FC*. If this condition is not fulfilled the resultant line profile is displaced and/or broadened. Three cases will be described: (1) The specimen surface has the proper curvature but is displaced or rotated from *FC*, (2) the surface is flat rather than curved, and (3) the specimen has low absorption and diffraction occurs from below as well as from the surface of the specimen.

Radial displacement

If the specimen is displaced a distance s along a radius vector and its curved surface remains parallel to *FC* the line profile is shifted toward larger reflection angles if the specimen surface lies within *FC* and towards smaller angles if it lies outside *FC*. This is often the source of the largest systematic angular error in powder diffractometry. The shift (see Table 1) is zero at 180°2θ, increases gradually with decreasing θ and then increases abruptly as 2θ approaches γ. Fig. 1 is a plot of the shift for several values of γ and was verified experimentally for $\gamma = 15°$ by placing shims of thickness $s = 0{\cdot}075$ and 0·125 mm between the specimen post and holder and measuring several peaks in the range 50° to 176°4θ. If s is small the line profile is not distorted and the magnitude of the shift is the same for all angular measures (peak, centroid, midpoint of chords); the intensity also remains the same. The ratio of the shifts (for the same s and R, and $\gamma = 15°$) $\Delta\theta_{RSD}$S–B/$c = 3{\cdot}8$ at 10°θ and 1·7 at 60° when $\Delta\theta$ is expressed in the same angular units. Although it is possible in theory to extend the S–B scanning range to smaller θ's the large radial displacement error would seriously limit the accuracy.

Angular displacement

If the specimen is rotated through an angle τ from *FC* the peak intensity decreases and the line breadth increases but the peak position remains essentially the same as shown in Fig. 2. This aberration may be understood as a convolution of a continuous series of radial specimen displacement aberrations resulting from the continuous variation in the amount of radial specimen displacement (from $+s$ to $-s$) as a function of speci-

* Research supported in part by Advanced Research Projects Agency and technically monitored by Air Force Office of Scientific Research under Contract AF49(638)-1234. Presented in part at American Crystallographic Association Meeting, Paper H1, 27 January 1967, Georgia Institute of Technology.

men length. Consequently the magnitude of the aberration should decrease with increasing diffraction angle (as in the conventional diffractometer) and this was confirmed experimentally. At low θ's, a small misset of τ causes a greater broadening than the same amount of 2:1 misset in the conventional diffractometer. For example, a misset $\tau = 0{\cdot}35°$ doubles the width and halves the peak intensity while a 1° misset of 2:1 in the conventional diffractometer is required to cause about the same distortion.

To avoid this defocusing the tolerance of the angular setting of the specimen must be of the order of a few hundredths of a degree. This could not be achieved easily by purely mechanical means and the procedure adopted was to 'peak' the reflection. After the approximate peak position was set manually, the specimen tilt was varied by means of a micrometer-lever until maximum intensity was achieved. For broad peaks it was necessary to converge on the proper setting by

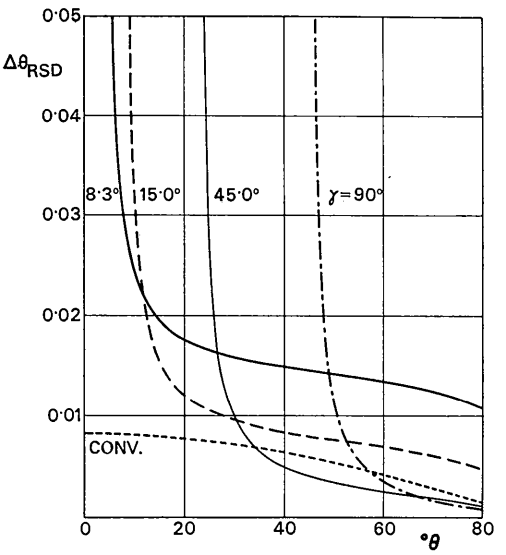

Fig. 1. Shift of peak, centroid or midpoint of chord in °θ caused by radial displacement of specimen surface $s = 0{\cdot}0254$ mm in S-B diffractometer, $R = 174$ mm. Shift in conventional diffractometer for same s and R shown by short-dash curve.

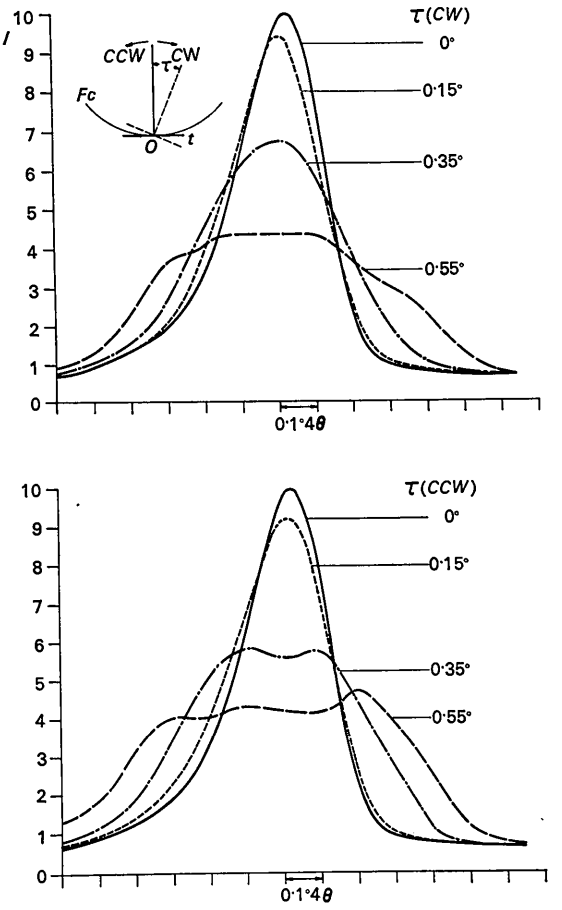

Fig. 2. Line profile distortion caused by small rotations τ (see insert) of curved specimen from focusing circle, silicon powder, 111 Cu $K\beta$.

Table 1. *Centroid shifts (in radians) arising from specimen aberrations*

Aberration	Seemann–Bohlin[a][b] $\Delta 4\theta$	Conventional[c] $\Delta 2\theta$	S–B/conventional $\Delta 2\theta$
Radial displacement	$\frac{s}{R}\,\frac{\sin 2\theta}{\sin\gamma\,.\,\sin(2\theta-\gamma)}$	$\frac{2s}{R_c}\cos\theta$	$\frac{\sin\theta}{2\sin\gamma\,.\,\sin(2\theta-\gamma)}$
Flat specimen[d]	$\frac{\alpha^2}{6}\,\frac{\sin 2\theta}{\sin\gamma\,.\,\sin(2\theta-\gamma)}$	$\frac{\alpha^2}{6}\cot\theta$	$\frac{\sin^2\theta}{\sin\gamma\,.\,\sin(2\theta-\gamma)}$ $(\alpha_{S-B}=\alpha_c)$
			$\frac{1}{4\sin\gamma\,.\,\sin(2\theta-\gamma)}$ $(l_{S-B}=l_c)$
Transparency			
$\mu h \to \infty$	$\frac{1}{\mu R}\,\frac{\sin 2\theta}{\sin\gamma+\sin(2\theta-\gamma)}$	$\frac{1}{2\mu R_c}\sin 2\theta$	$\frac{1}{\sin\gamma+\sin(2\theta-\gamma)}$
$\mu h \to 0$	$\frac{h}{2R}\,\frac{\sin 2\theta}{\sin\gamma\,.\,\sin(2\theta-\gamma)}$	$\frac{h}{R_c}\cos\theta$	Same as radial displacement

(*a*) Segmüller (1957).
(*b*) Kunze (1964).
(*c*) Wilson (1963).
(*d*) α in radians.

alternately adjusting the detector and specimen positions. The micrometer setting for $\tau = 0°$ (specimen surface coincident with *FC*) may differ for different specimens, for it is dependent on the machining accuracy of the curved specimen holder and the specimen preparation. In practice, it was found that τ generally changed by less than 0·05° in changing specimens.

Flat specimen aberration

One of the important advantages of the S–B geometry is that the radius of the focusing circle is constant and hence a specimen with one radius of curvature may be used for all diffraction angles. If a flat specimen must be used the line profiles will be asymmetrically broadened and shifted by a greater amount than in the conventional diffractometer. The high angle side of the profile is not affected but the low angle side is stretched out causing the centroid to be shifted more than the peak.

The expression for the centroid shift is given in Table 1 and is plotted in Fig. 3. The shift is proportional to α^2 and decreases with increasing θ. This aberration may be interpreted as a continuous series of radial displacements of the specimen surface from the focusing circle in which s varies with irradiated specimen length l. In the S–B, $l_{S-B} = 2\alpha R$ and in the conventional $l_c = \alpha R_c / \sin\theta$; the ratio $l_{S-B}/l_c = 2\sin\theta$ (for the same α and R) and varies from 0·3 at 10°θ to 1·7 at 60°. If the same l's were used in both diffractometers, the ratio of the centroid shifts would vary from 11·1 at 10°θ to 1·0 at 60°. If the same α's were used, the ratio would vary from 1·3 at 10°θ to 3·0 at 60°.

The extent of the flat specimen aberration is shown in Fig. 4. The same flat specimen was used for all recordings, the α's were selected to give approximately the same l's for both diffractometers, and the peak intensities were normalized to allow easy comparison

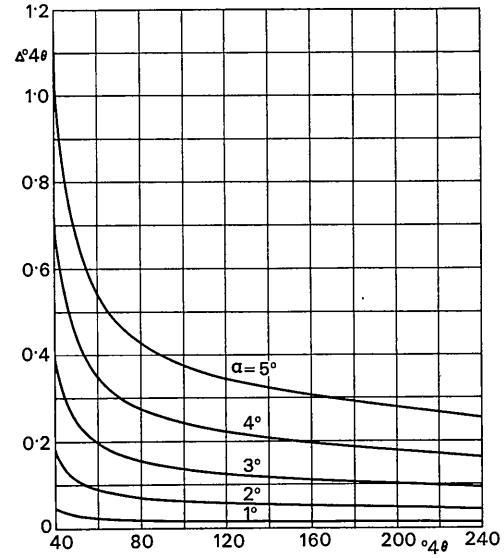

Fig. 3. Shift of centroid in °4θ caused by use of flat specimen in S–B, $\gamma = 15°$, $R = 174$ mm.

of the shapes. The calculated centroid shift in the same angle units (°2θ) for the silicon powder 111 Cu $K\beta$ reflection at 25·6°2θ is 6 times greater for α_{S-B} 4·1°, l_{S-B} 24·9 mm than for α_c 1·7°, l_c 23·2 mm [compare Fig. 4(*a*) and (*b*)]. The shift of the 422 Cu $K\alpha_{1,2}$ profile in the S–B at 88°2θ is less than one-half the shift of 111 using the same α's, as shown in Fig. 4. The bumpy low angle side of some of the S–B profiles is not an artifact and was reproducible. Profiles from a specimen with intermediate curvature ($R = 504$ mm) had about one-half the distortion of those from flat specimens.

The integrated line intensity with background subtracted was proportional to α. The net peak intensities depended on the extent of the aberration; for example they were nearly the same for $\alpha = 2·3°$ and 4·1° at 25°2θ.

Transparency

X-rays diffracted at a depth x below the specimen surface are attenuated by the factor

$$\exp -[\mu x \csc\gamma + \mu x \csc(2\theta - \gamma)] \qquad (1)$$

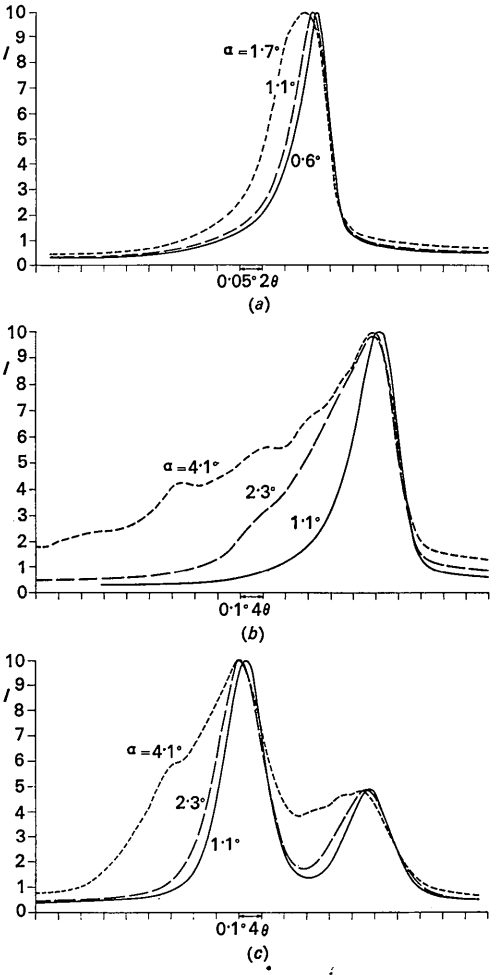

Fig. 4. Flat specimen aberration. (*a*) Conventional diffractometer, (*b*) and (*c*) S–B diffractometer. (*a*,*b*) Silicon powder 111 Cu $K\beta$, (*c*) silicon 422 Cu $K\alpha_{1,2}$. Peak intensities normalized; net peak intensities were 6740, 7930 and 7900 c.sec^{-1} in order of increasing α in (*b*).

where μ is the observed linear absorption coefficient. The observed intensity is then reduced by the absorption factor

$$A(\mu,h)=\frac{1}{S_0}\int \exp(-\mu g h)dv \qquad (2)$$

where h = specimen thickness

S_0 = cross-section of incident beam = $2\alpha RL \sin\gamma$;
L = axial length
g = $\csc\gamma+\csc(2\theta-\gamma)$
v = diffracting volume

and the integration is over the irradiated specimen volume. The integral was evaluated following the procedure Wilson (1963) used for the conventional diffractometer and the resultant expression is

$$A(\mu,h)=\frac{\csc\gamma}{\mu f g}\left\{\left[2f-\frac{1}{\mu g}\right]\right.$$
$$\left.[1-\exp(-\mu g h)]+[h\exp(-\mu g h)]\right\} \qquad (3)$$

where $f=\alpha R\sin\gamma\,.\csc 2\theta\,.\sin(2\theta-\gamma)$; h must be replaced by $2f$ if the latter is smaller. Equation (3) may be simplified for the two limiting cases, highly absorbing thick specimens $\mu h\to\infty$ and low absorbing thin specimens $\mu h\to 0$, as shown in Table 2.

It was assumed in the derivation that the angular apertures of the incident and diffracted beams were equal. This is justified in the S–B geometry where the same specimen length is irradiated at all diffraction angles. In the case of very low absorbing specimens the length of beam reflected and detected is determined by the specimen length rather than by the antiscatter slit as may occur in certain cases in the conventional diffractometer (Milberg, 1958; Levy, Agron & Danford, 1959).

The intensity for the case $\mu h\to 0$ was measured with a number of 0·0031 cm thick beryllium foils selected for uniformity of thickness and X-ray transmission. The rolling of the foils during fabrication resulted in a strong preferred orientation of the basal planes parallel to the surface and hence the 00.2 reflection was intense. The foils were clamped against the curved surface of a modified specimen holder and shims were used to bring the top surface into coincidence with *FC*. The data, summarized in Table 3, show excellent agreement of observed and calculated integrated line intensities.

The specimen transparency is also a source of asymmetric line broadening and shifts the profile to smaller θ's. Fig. 5(*a*) shows profiles of the same set of beryllium foils described above obtained with the conventional diffractometer and Fig. 5(*b*) with the S–B; the peak intensities were normalized. Although the profiles in Fig. 5(*a*) have a small amount of additional 'flat specimen' broadening because the curvature was 174 mm instead of the optimum value of 223 mm, the profiles are narrower than those in Fig. 5(*b*). The line profile broadening arising from specimen transparency may

Table 2. *Geometrical dependent factors for calculating integrated intensity*

μ_a linear absorption coefficient of air.
μ linear absorption coefficient of specimen.
R_T radius of X-ray tube.

Factor	Seemann–Bohlin[a][b]	Conventional[c]	S–B/Conventional
Chord length	$\frac{L_{RS}}{4\pi R\sin(2\theta-\gamma)\,.\sin 2\theta}$	$\frac{L_{RS}}{2\pi R_c\sin 2\theta}$	$\frac{1}{2\sin(2\theta-\gamma)}$
Air transmission	$\exp\{-\mu_a[2R\sin\gamma+2R\sin(2\theta-\gamma)-R_T]\}$	$\exp\{-\mu_a[2R_c-R_T]\}$	$\exp\{-2\mu_a R[\sin\gamma+\sin(2\theta-\gamma)-1]\}$
Transparency			
$\mu h\to\infty$	$\frac{\sin(2\theta-\gamma)}{\mu[\sin\gamma+\sin(2\theta-\gamma)]}$	$\frac{1}{2\mu}$	$\frac{2\sin(2\theta-\gamma)}{\sin\gamma+\sin(2\theta-\gamma)}$
$\mu h\to 0$	$\frac{h}{\sin\gamma}$	$\frac{h}{\sin\theta}$	$\frac{\sin\theta}{\sin\gamma}$

(*a*) Segmüller (1957).
(*b*) Kunze (1964).
(*c*) Wilson (1963).

Table 3. *Transparency line profile data, beryllium foils,* (00·2) Cu *Kβ*

Profile [Fig. 5(*b*)]	Number of foils	h (mm)	$W_{1/2}$* (°4θ)	P† (c.sec^{-1})	I‡ obs.	I‡ calc.
a	1	0·031	0·20	2400	0·12	0·12
b	2	0·062	0·25	4000	0·23	0·24
c	4	0·124	0·37	5400	0·45	0·45
d	6	0·186	0·44	6800	0·65	0·65
e	10	0·310	0·68	7300	1·00	1·00

* Width at one-half peak height above background.
† Peak counting rate above background.
‡ Integrated line intensity above background, normalized; $\mu=2{\cdot}1$ cm^{-1} used in calculation.

be explained qualitatively in terms of radial specimen displacement. In Fig. 5(*a*) the width $W_{\frac{1}{2}}$ of the profiles at one-half peak height increased 0·019°2θ per foil compared with 0·015° calculated from radial specimen displacement using a value of s equal to the foil thickness. The comparable values for the S–B profiles of Fig. 5(*b*) were $W_{\frac{1}{2}}=0{\cdot}053°4\theta$ and the calculated value was 0·055°.

Expressions for the centroid shift resulting from specimen transparency are given in Table 1; for the case $\mu h \to 0$ the geometric term is the same as for radial displacement. Fig. 6(*a*) is a plot of the centroid shift in the S–B when $\mu h \to \infty$ and Fig. 6(*b*) for $\mu h \to 0$; the latter is much larger and more θ-dependent. The shift when $\mu h \to 0$ is 3·8 times larger in the S–B than in the conventional diffractometer at 10°θ and is 1·7 times larger at 60°.

Similar data were obtained with various thickness diamond specimens cemented to the under surface of a single beryllium foil. However, the data could be interpreted only semi-quantitatively because of difficulties in preparing very thin uniform specimens and in measuring their thickness accurately.

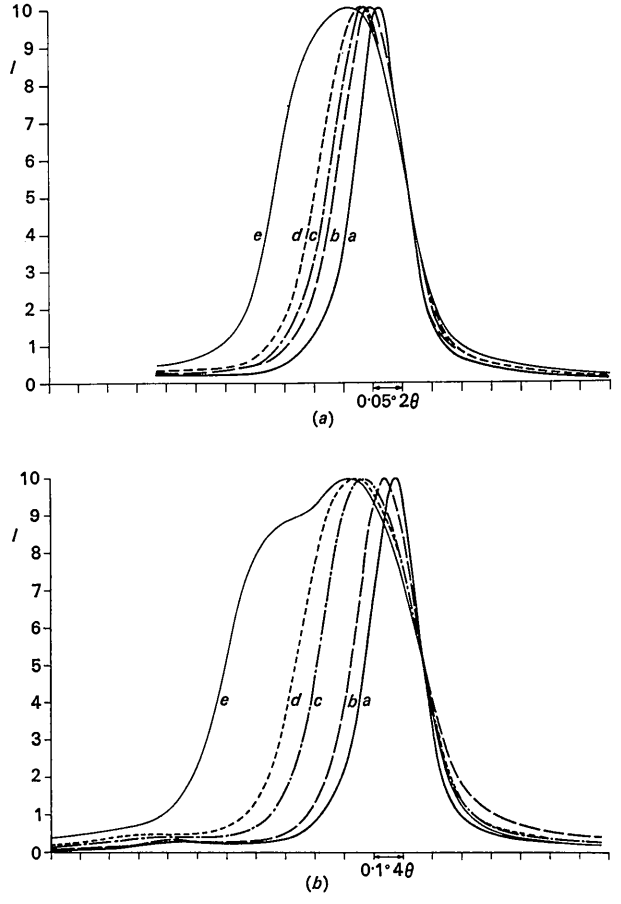

Fig. 5. Transparency aberration, $\mu h \to 0$, curved beryllium foils each 0·031 mm thick, a to $e=1,2,4,6$ and 10 foils, peak intensities normalized, 00.2 Cu $K\beta$, 22·9°θ. (*a*) Conventional and (*b*) S–B diffractometer.

Preferred orientation

Since the orientation of the reflecting plane H with respect to the specimen surface is different for the two diffractometers this might be a basis for determining if preferred orientation occurred in a specimen preparation by comparing the relative intensities obtained with both methods. The S–B instrument used in this study had a θ_H range of 11° to 54° and $\gamma=15°$ so that the inclination of H to the specimen surface varied from $\beta_H=-4°$ to $+39°$ whereas $\beta_H=0°$ for all θ's in the conventional diffractometer. Since the relative intensities of the basal and pinacoid reflections are most affected by preferred orientation and these are often the larger spacings occurring in the range 11° to 20°θ using Cu $K\alpha$ radiation, the β_H then varies only from $-4°$ to $+5°$ which is too small a difference from the conventional diffractometer to be useful in this determination. Increasing γ changes the β_H range but increases the minimum value of θ_H. In addition, in the variable receiving aperture S–B it would be necessary first to correct the intensities for ε^*_{S-B} (Parrish & Mack, 1967).

Air absorption losses

The X-ray path length in the S–B varies with diffraction angle and hence the air absorption losses vary accordingly. The incident path length in air is $2R\sin\gamma - R_T$, where R_T is the radius of the X-ray tube; the diffracted ray path varies as $2R\sin(2\theta-\gamma)$ and is a maximum at $180°+2\gamma$. In the present S–B instrument the transmission of Cu $K\alpha$ radiation in the entire air path decreases from 90% at 40°4θ to 62% at 210° and for Cr $K\alpha$ radiation varies from 73% to 23% at the same angles. In the conventional diffractometer the path length is constant and the transmission of Cu $K\alpha$ is 69% and of Cr $K\alpha$ 32% for the same goniometer radius as the S–B. These values were calculated using a linear absorption coefficient of air μ_a without moisture at 20°C and 760 mmHg=0·0119 cm^{-1} for Cu $K\alpha$ and 0·0364 for Cr $K\alpha$.

Chord length of receiving slit

In the conventional diffractometer the chord length of the powder ring intercepted by the axial length of the receiving slit is $L_{RS}/2\pi R\sin 2\theta$, which is nearly uniform from 30° to 60°θ and increases gradually from 30° to 10°θ. In the S–B the chord length is $L_{RS}/[4\pi R\sin(2\theta-\gamma)\times\sin 2\theta]$ and has a greater angular dependence. The increase below 30°θ is much greater for the S–B and is the most significant factor in the greater intensity at small θ's.

Intensity

The diffracted intensity is proportional to

$$I_0 A(\mu,h)TB \qquad (4)$$

where I_0 is the incident intensity for the given X-ray tube operating conditions and is proportional to α, δ

and the axial length L of the incident beam assembly, $A(\mu,h)$ is the specimen absorption factor given by equation (3), T the transmission of the entire X-ray air path and B the chord length of the diffracted cone intercepted by L_{RS}. Expressions for each of these factors for the S–B and conventional diffractometers are given in Table 2. The ratio of integrated intensities observed with the variable ε^* S–B and the conventional diffractometer is

$$\frac{I(\varepsilon^*_{S-B})}{I_c}=\frac{\alpha\delta L_{S-B}}{\alpha\delta L_c}\,\frac{\exp-\{2\mu_a R[\sin\gamma+\sin(2\theta-\gamma)-1]\}}{\sin\gamma+\sin(2\theta+\gamma)}. \tag{5}$$

This ratio assumes the same goniometer radii, receiving slit widths, X-ray tube operating conditions and scanning rates and is appropriate for a highly absorbing specimen. To obtain the ratio for the constant ε S–B, equation (5) must be multiplied by $2\sin(2\theta-\gamma)$. The ratio is plotted in Fig. 7 as a solid line for ε^*_{S-B} and as a dashed line for ε_{S-B}; the values used in the calculation were $\alpha_{S-B}=4{\cdot}1°$, $\alpha_c=1{\cdot}1°$, the same values for δ and L, $R=R_c=174$ mm, $\gamma=15°$ and $\mu_a=11{\cdot}9$-cm^{-1} for Cu $K\alpha$ radiation. An expression similar to equation (5) has been given by Segmüller (1957) and is implicit in the treatment given by Kunze (1964).

To verify equation (5) the ε^* S–B and conventional diffractometers were carefully aligned at opposite windows of a copper fine-focus X-ray tube. The same counting circuit system and detector were used for all measurements by transferring the scintillation counter. These precautions ensured that the experimental parameters such as X-ray tube intensity and the detector sensitivity were maintained constant. Two specimens each of silicon and lead nitrate powder, particle size $<25\mu$, were used. The specimen radius of curvature was 174 mm for the S–B and 504 mm for the conventional diffractometer; the latter is the correct curvature only at $20°2\theta$ but does not influence the integrated intensity measurements. Four lines were measured for each specimen: silicon 111β, 220α, 311α and

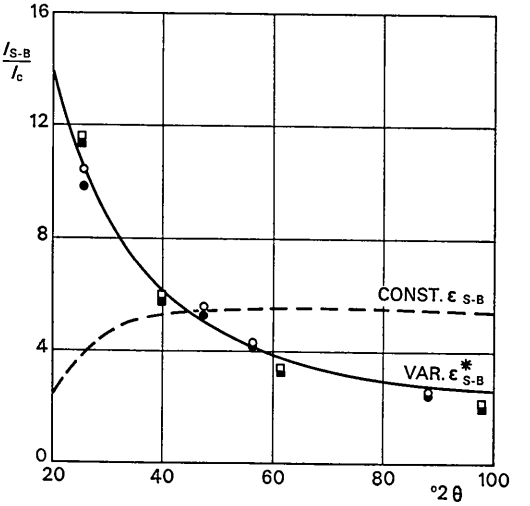

Fig. 7. Calculated ratio of net integrated intensities of S–B to conventional diffractometer for variable aperture ε^* (solid line) and constant aperture ε (dashed line). Observed ratios for ε^*: silicon, open circles $W_{RS}=0{\cdot}076$ mm, filled circles $W_{RS}=0{\cdot}254$ mm; lead nitrate, open squares $W_{RS}=0{\cdot}076$ mm, filled squares $W_{RS}=0{\cdot}254$ mm.

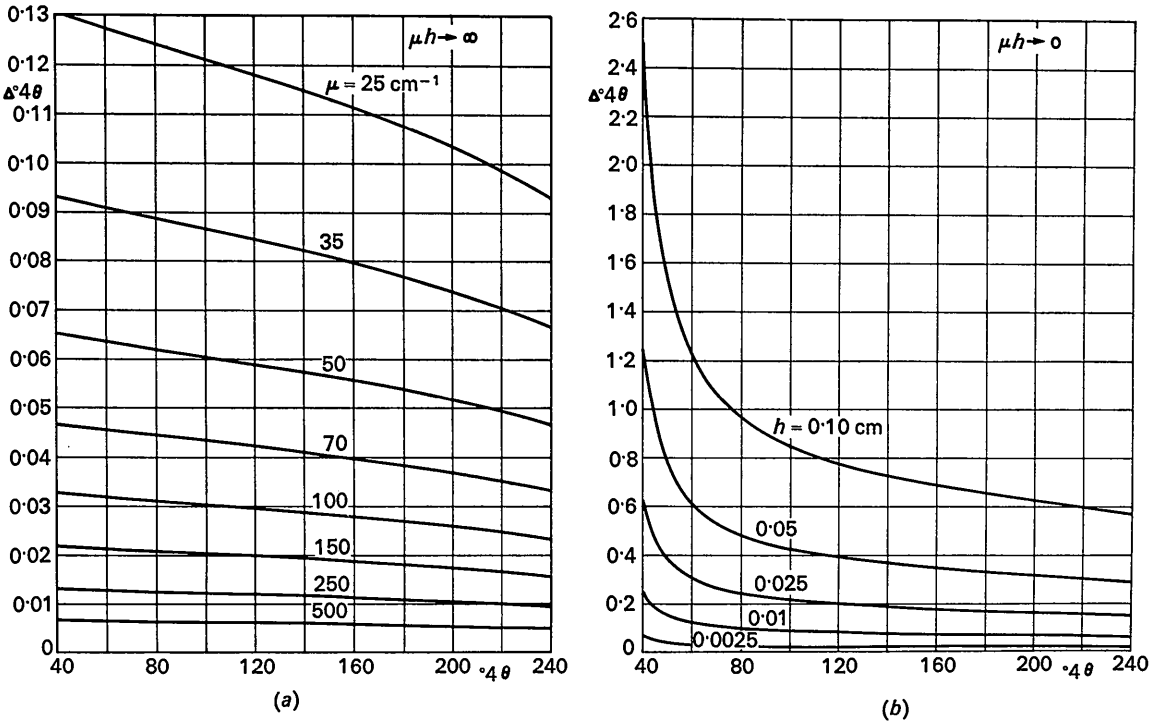

Fig. 6. Shift in centroid in $°4\theta$ caused by specimen transparency in S–B, $\gamma=15°$, $R=174$ mm; (*a*) $\mu h\to\infty$, (*b*) $\mu h\to 0$.

422α; lead nitrate 210α, 222α, 511α and 731α; and two receiving slit widths, 0·075 and 0·25 mm, were used. The scanning rate was $\frac{1}{16}°\theta$ min^{-1} and the scanning range was controlled accurately by a preselected counting time interval. The number of counts accumulated in the scaling circuit minus the background determined at both ends of the profile was taken as the integrated line intensity. The experimental data check well with equation (5) and show the large θ-dependence of the integrated intensity ratio.

Comparison of diffractometers

Powder patterns of curved quartz specimens obtained with variable ε^* and constant ε S–B and conventional diffractometers using the experimental arrangement described above are shown in Fig. 8. The observed relative peak intensities of the $K\alpha$, on the basis of 10.1 = 100, were

	11.0	11.2	12.1	13.1
ε^*_{S-B}	7	9	5	0·7
ε_{S-B}	8	14	9	1·5
ε_c	7	13	8	1·4

The relative peak intensities in the conventional diffractometer are not usually corrected for resolution and errors may arise in comparing peak heights of $K\alpha$ doublets which have different degrees of resolution. The relative peak intensities for the constant ε S–B and conventional diffractometers are in good agreement but the variable ε^* S–B shows a large systematic error as a result of the varying resolution. The latter data must be corrected in order to compare them with standard powder intensity data such as in the ASTM Index.

The peak intensities with the variable ε^* S–B vary from 7·1 times higher than the conventional diffractometer at 26·6°2θ to 3·5 at 83·7°. The peak intensity ratio for the constant ε S–B was 3·8 at 26·6° and remained nearly constant at about 5·4 above 36°; these values check well with the calculated integrated intensity ratios shown in Fig. 7. These results are to be expected because the receiving aperture is the same in both cases and hence the resolution is approximately the same.

The results given by Das Gupta, Schnopper, Metzger & Shields (1966) could not be compared with our data because the experimental conditions were markedly different. Baun & Renton (1963) compared the Cu $K\alpha$ 400 profiles of a molybdenum specimen using both types of diffractometer and state the S–B has better resolution. This interpretation is not correct because the *angular* separation is the same since the S–B scale is in °4θ. The flat specimen aberration is small at large diffraction angles and their peak-to-background ratio was lower than that of the conventional diffractometer. We were unable to verify the expressions given by Dunne (1965).

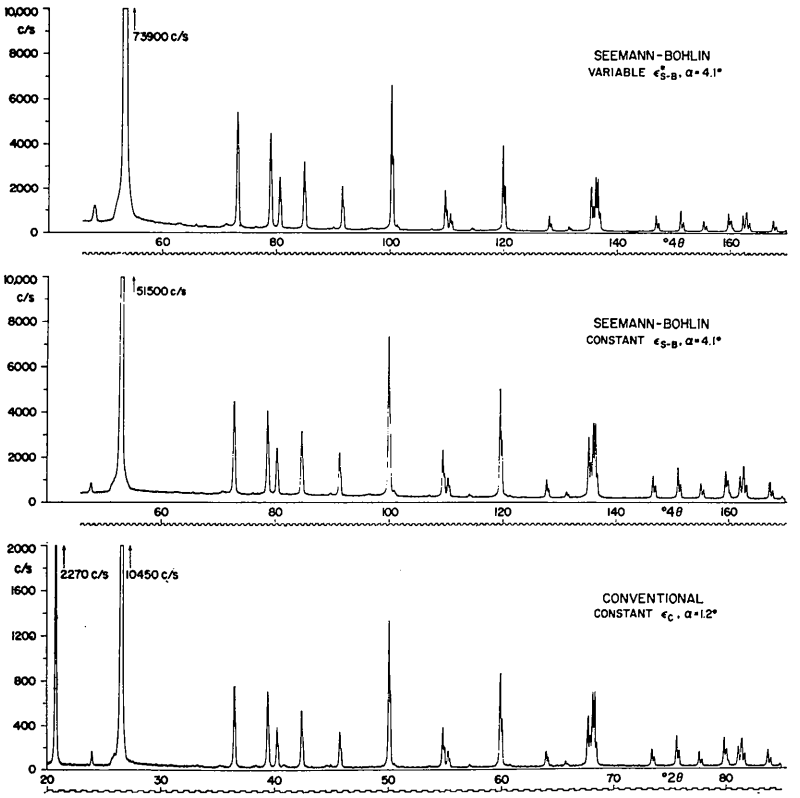

Fig. 8. Quartz powder patterns obtained with S–B and conventional diffractometers using the same experimental conditions. Top recording: W_{RS} = 0·254 mm; middle: ε_{S-B} = 0·08°2θ; bottom: W_{RS} = 0·254 mm, ε_c = 0·08°2θ.

The relative merits of the S–B and conventional diffractometers may be evaluated as follows. The S–B has approximately five times higher intensity, the flat specimen aberration is eliminated for all diffraction angles by a single curvature, the stationary specimen simplifies the design and use of devices for varying the environmental conditions, and several detectors may be used simultaneously for dynamic studies or for reducing the scanning time. The disadvantages inherent in the geometry are: the angular range is limited and for the instrument used (Parrish, Mack & Vajda, 1967) the d-range is only 3·87 Å to 0·95 Å with Cu $K\alpha$ radiation, the inaccessible zero angle makes it necessary to use standard substances for angular calibration, extreme care must be used in specimen preparation to avoid intensity errors arising from surface roughness and large displacement errors at small diffraction angles, rotating flat specimens to reduce the effect of crystallite size statistics can be used only with small angular apertures thus reducing the intensity gain, the variation in the angular resolution in the variable ε^* S–B requires correction of the relative intensities. The conventional diffractometer is thus a more versatile and accurate general purpose instrument while the S–B should be utilized for certain special applications.

We are indebted to Mrs P. Harnack for technical assistance and Miss H. P. Goodman and Mrs M. L. Bonney for preparing the illustrations.

References

BAUN, W. L. & RENTON, J. J. (1963). *J. Sci. Instrum.* **40**, 498.
DAS GUPTA, K., SCHNOPPER, H. W., METZGER, A. E. & SHIELDS, A. R. (1966). *Advanc. X-ray Anal.* **9**, 221.
DUNNE, J. A. (1965). Techn. Memo. 33-218, p. 129, Jet Propulsion Lab., Pasadena, Calif., 1 June.
KUNZE, G. (1964). *Z. angew. Phys.* **17**, 412; **17**, 522; **18**, 28.
LEVY, H. A., AGRON, P. A. & DANFORD, M. D. (1959). *J. Appl. Phys.* **30**, 2012.
MILBERG, M. E. (1958). *J. Appl. Phys.* **29**, 64.
PARRISH, W. (1965). *X-ray Analysis Papers*. Eindhoven: Centrex Publishing Co.
PARRISH, W. & MACK, M. (1967). *Acta Cryst.* **23**, 687.
PARRISH, W., MACK, M. & VAJDA, I. (1967). *Norelco Reporter*, **14**, 56.
SEGMÜLLER, A. (1957). *Z. Metallk.* **48**, 448.
SEGMÜLLER, A. & WINCIERZ, P. (1959). *Arch. Eisenh.* **30**, 577.
WILSON, A. J. C. (1963). *Mathematical Theory of X-ray Powder Diffractometry*. Eindhoven: Philips Technical Library.

Acta Cryst. (1967). **23**, 700

The Atomic Radial Distribution Function in Amorphous Selenium

BY ROGER CHANG AND PAUL ROMO

North American Aviation Science Center, Thousand Oaks, California, U.S.A.

(*Received* 12 *April* 1967)

The atomic radial distribution curves for vitreous selenium quenched from two melt temperatures, 700 and 775 °K, were evaluated from X-ray diffraction measurements using Cu K and Mo K radiations and balanced filters. The general features of the radial density function are similar to those published in the literature. A consideration of the fine details of the radial density function suggests that quenching from different melt temperatures yields vitreous selenium of slightly different packings of the atoms at larger radial distances than the nearest neighbor separation of 2·3 Å. A quantitative correlation between the radial density function and the actual intermolecular structure of the material must await, however, better low-angle intensity data and accurate extension of the intensity curve to larger S values than used in this study.

Introduction

Earlier studies of the atomic radial distribution function in amorphous selenium have been reported by Richter and other investigators using X-ray diffraction (Richter & Herre, 1958; Lark-Horovitz & Miller, 1937; Hendus, 1942). More recently Henninger, Buschert & Heaton (1967) reinvestigated the problem with both X-ray and neutron diffraction. Henninger and coworkers concluded that the intensity function can largely be accounted for by considering only two interatomic distances between the first and second nearest neighbors along the c-axis chain structure of hexagonal crystalline selenium and that the spiral structure persists in the amorphous state with nearly unchanged geometry out to the second nearest neighbors but in random orientations.

The elastic and anelastic properties (in the megacycle frequency range), viscosity, and electrical resistivity of vitreous selenium near its glass transition temperature were measured as a function of the quench (or melt) temperature by Graham & Chang (1965). The meas-